Singlet dark matter in the SU(6)/SO(6) composite Higgs model

Haiying Cai, Giacomo Cacciapaglia

Singlet dark matter in the SU(6)/SO(6) composite Higgs model

Haiying Cai[1,2,*] and Giacomo Cacciapaglia[3,4,†]

[1]*Asia Pacific Center for Theoretical Physics, Pohang, Gyeongbuk 790-784, Republic of Korea*
[2]*Tsung-Dao Lee Institute, and School of Physics and Astronomy, Shanghai Jiao Tong University, Shanghai 200240, China*
[3]*Institut de Physique des Deux Infinis de Lyon (IP2I), CNRS/IN2P3 UMR5822, 4 rue Enrico Fermi, 69622 Villeurbanne Cedex, France*
[4]*Université Claude Bernard Lyon 1, Université de Lyon, 92 rue Pasteur, 69361 Lyon Cedex 07, France*

(Received 16 July 2020; accepted 8 February 2021; published 2 March 2021)

Singlet scalar dark matter can naturally arise in composite Higgs models as an additional stable pseudo-Nambu-Goldstone boson. We study the properties of such a candidate in a model based on SU(6)/SO(6), with the light quark masses generated by 4-fermion interactions. The presence of nonlinearities in the couplings allows us to saturate the relic density for masses $400 < m_{\rm DM} < 1000$ GeV, and survive the bound from direct detection and indirect detection. The viable parameter regions are in reach of the sensitivities of future upgrades, like XENONnT and LZ.

DOI: 10.1103/PhysRevD.103.055002

I. INTRODUCTION

The standard cosmology model, "ΛCDM" based on a flat prior, can well describe an expanding universe from the early to late times. The combination of radiation, matter, and dark energy determines the Hubble expansion $H(t) = \dot{a}(t)/a(t)$ as governed by the Friedmann equations. According to astrophysical measurements, the present Universe consists of roughly 30% matter and 70% dark energy after the dark age and large scale structure emergence [1]. However, the density of baryonic matter today is $\Omega_b h^2 \sim 0.02$, comprising only a small portion of the total matter. Thus, the remaining 85% of the total matter is made of a dark component, expected to be distributed as spherical halos around Galaxies. Despite the convincing evidences for dark matter (DM) from various sources, such as the galaxy rotation curves, gravitational lensing and observations of cosmic microwave background (CMB), the particle identity of DM has not been identified yet. In the Standard Model of particle physics (SM), the only candidates, neutrinos, are too light and have too small a relic density to account for the observation. Therefore, many theories beyond the Standard Model (BSM) have been proposed, with the most popular ones advocating weakly interacting massive particles (WIMPs) stabilized by a discrete symmetry: this scenario can naturally provide a suitable DM candidate thanks to the thermal decoupling.

One of the possibilities is the Higgs mediated singlet scalar DM model. Without consideration for the naturalness of the light scalar mass, the DM physics is simply described by two free parameters: the mass m_S and Higgs coupling to the singlet scalar λ_{hSS} [2–4]. Because of the small parameter space, this model has high predictive power. The dominant DM annihilation channels, which determine the thermal relic density, are as follows: for $m_S < m_W$, a DM pair mainly annihilates into $\bar{b}b$, while in the high mass region its annihilation cross section into WW, ZZ, and hh turns to be very effective. However, the viable parameter space for the model is tightly squeezed [5,6] since the λ_{hSS} coupling is subject to strong constraints from direct detection experiments, e.g., Xenon1T [7], PandaX [8], and LUX [9], as well as by the bounds on the Higgs invisible decay width and the upper bounds on events with large missing energy at the LHC experiments. In this work we plan to investigate this scenario in the context of a composite Higgs model (CHM) that enjoys an underlying gauge-fermion description and can be UV completed. The scalar DM candidate emerges as a pseudo-Nambu-Goldstone boson (pNGB) together with the Higgs boson itself. In our scenario, the composite nature of both DM and the Higgs boson can substantially modify the DM couplings to the SM states and alter the relative importance of various annihilation channels. This is mainly due to the presence of higher order couplings, generated by nonlinearities in the pNGB couplings, which can enhance the annihilation cross sections while the coupling to the Higgs (constrained by Direct Detection) is small. This kind of scenario was first

*haiying.cai@apctp.org
†g.cacciapaglia@ipnl.in2p3.fr

proposed in Ref. [10] in the context of the minimal coset $SU(4)/Sp(4)$, however the scalar candidate is allowed to decay if a topological anomaly is present, like is always the case for models with a microscopic gauge-fermion description [11]. Thus, it is necessary to work in scenarios with larger global symmetries, which allows for singlet scalar states which do not couple via the topological term, and can therefore be stable. Also, in Ref. [12] it has been pointed out that the DM has dominant derivative couplings to the Higgs, which again ensures the suppression of direct detection rates [13]. However, the nature of the couplings is basis dependent, as one can always choose a basis for the pNGBs where the derivative coupling is absent [14]. In this paper we will work in this basis.

The CHM we studied is based on the coset $SU(6)/SO(6)$, which enjoys a microscopic description with underlying fermions transforming in a real representation of the confining gauge group [15]. Top partial compositeness can also be implemented along the lines of Ref. [16]. The pNGB sector is similar to the $SU(5)/SO(5)$ model [17], which is the minimal realistic coset in the $SU(N)/SO(N)$ family: the pNGBs include a bitriplet of the custodial $SU(2)_L \times SU(2)_R$ global symmetry, like the Georgi-Machacek (GM) model [18]. However, unlike the GM model, the direction inside the bitriplet that does not violate the custodial symmetry is *CP* odd, thus it usually cannot develop a vacuum expectation value in a *CP* conserving theory. On the other hand, the interactions of fermions to the composite sector typically induce a tadpole for the custodial triplet component, thus generating unbearable contributions to the ρ parameter. For the top, coupling to composite fermions in the adjoint representation of SU(5) allows us to avoid this issue [19]. In our model, the adjoint of SU(6) serves the same purpose, while the masses of the light fermions can be generated by other mechanisms. This results in a violation of custodial symmetry of the order of m_b^2/m_h^2, thus being small enough to evade precision bounds, as we demonstrate in this paper. The extension of the model to SU(6) also contains a second Higgs doublet and a singlet, which can be protected by a $\mathbb{Z}_2$ symmetry for suitable couplings of the top quark [15]. For other examples of CHMs with DM, see Refs. [20–27].

In this work, we investigate the properties of the singlet, $\mathbb{Z}_2$-odd, pNGB as a candidate for dark matter. We find that, notwithstanding the presence of additional couplings, the model is tightly constrained, especially by direct detection. The small parameter space still available will be tested by the next generation direct detection experiments, with DM masses in the 400 to 1000 GeV range.

II. THE MODEL

The main properties of the low energy Lagrangian associated to this model have been studied in detail in Ref. [15], where we refer the reader for more details. In this section, we will briefly recall the main properties of the pNGBs, and discuss in detail how custodial violation is generated via the masses of the light SM fermions. The latter point was not discussed in the previous work. Following Refs. [15,19], we will embed the SM top fields in the adjoint representation of the global SU(6): this is the only choice that allows for vanishing triplet VEV, thus preserving custodial symmetry. For the light fermions, we will add direct four-fermion interactions to generate effective Yukawa couplings to the composite Higgs sector.

TABLE I. Quantum numbers of the 20 pNGBs in terms of the EW and custodial symmetries. Here, the pNGB are defined around the EW-preserving vacuum $\Sigma_{\rm EW}$. The last column indicates the $\mathbb{Z}_2$ protecting the DM candidate, as defined in the text.

	$SU(2)_L \times U(1)_Y$	$SU(2)_L \times SU(2)_R$	$\mathbb{Z}_2$
H_1	$(2, \pm 1/2)$	$(2, 2)$	$+$
H_2	$(2, \pm 1/2)$	$(2, 2)$	$-$
Λ	$(3, \pm 1)$	$(3, 3)$	$+$
φ	$(3, 0)$		
η_1	$(1, 0)$	$(1, 1)$	$+$
η_2	$(1, 0)$	$(1, 1)$	$-$
η_3	$(1, 0)$	$(1, 1)$	$+$

For a start, we recall the structure of the 20 pNGBs generated in this model. To do so, it is convenient to define them around a vacuum that preserves the EW symmetry, incarnated in a 6×6 symmetric matrix $\Sigma_{\rm EW}$ (for the explicit form, see Ref. [15]). The pNGBs can thus be classified in terms of the EW gauge symmetry $SU(2)_L \times U(1)_Y$, and of the global custodial symmetry envelope $SU(2)_L \times SU(2)_R$, which needs to be present in order to preserve the SM relation between the Z and W masses [28]. These quantum numbers are given in Table I.

A nonlinearly transforming pNGB matrix can be defined as

$$\Sigma(x) = e^{i\frac{2\sqrt{2}}{f}\Pi(x)} \cdot \Sigma_{\rm EW}, \tag{1}$$

where $\Pi(x)$ contains the pNGB fields [15]. We can now define a $\mathbb{Z}_2$ transformation that is from a broken global $U(1)$:

$$\Omega_{\rm DM} = \begin{pmatrix} \mathbb{1}_2 & & \\ & \mathbb{1}_2 & \\ & & \sigma_3 \end{pmatrix}, \quad \Omega_{\rm DM}\Sigma(x)\Omega_{\rm DM} = \Sigma'(x), \tag{2}$$

where $H_2 \to -H_2$ and $\eta_2 \to -\eta_2$ in $\Sigma'(x)$. Thus, they are the $\mathbb{Z}_2$-odd states, while all the other pNGBs are even, as indicated in the last column in Table I. This parity commutes with the EW and custodial symmetries, and with a suitable choice of the top couplings in the adjoint spurion [15], thus it can remain an exact symmetry of this model. This $\mathbb{Z}_2$ with $\det \Omega_{\rm DM} = -1$ is a remnant of a $U(1)$ global symmetry, that protects DM candidates from the topological anomaly interaction in the microscopic

gauge-fermion theory and uniquely determines the parity assignment in Table I. The DM candidates, therefore, can be either the singlet pseudoscalar η_2 or the component field A_0 in the second doublet H_2, which are both CP odd. Note that the CP-even components of $H_{\pm,0}$ are always heavier and will eventually decay into the lightest $\mathbb{Z}_2$-odd particle.

To study the properties of the DM candidate, we need to introduce the effects due to the breaking of the EW symmetry. The latter is due to some pNGBs acquiring a VEV: this effects can be introduced as a rotation of the vacuum by a suitable number of angles. In our case, as we want to preserve the dark $\mathbb{Z}_2$, we will assume that only H_1 will acquire a VEV, and check the consistency of this choice *a posteriori* when studying the potential for the pNGBs. For generality, we also introduce a VEV for the custodial triplet, corresponding to $\lambda_0 = -\frac{i}{\sqrt{2}}(\Lambda_0 - \Lambda_0^*)$. The rotation allows us to define a new pNGB matrix,

$$\Sigma_{\alpha,\gamma}(x) = U(\alpha,\gamma)\cdot\Sigma(x)\cdot U^T(\alpha,\gamma), \tag{3}$$

where

$$U(\alpha,\gamma) = e^{i\gamma\sqrt{2}S_8}\cdot e^{i\alpha\sqrt{2}X_{10}}\cdot e^{-i\gamma\sqrt{2}S_8}. \tag{4}$$

This rotation can be interpreted as follows: the exponential containing α is generated by a VEV for H_1, aligned with the broken generator X_{10}; then, we operate a rotation generated by the unbroken generator S_8 that misaligns the VEV along the direction of λ_0 by an angle γ. As the effect of the VEVs is an SU(6) rotation of the pNGB matrix, the couplings among pNGBs are unaffected as the chiral Lagrangian is invariant under such type of rotation: thus, no derivative couplings between one Higgs boson with two DM states is generated in this basis. Here we normalize f such that $v = 246\ \text{GeV} = f\sin\alpha$ for $\gamma = 0$.

The precise value of the two angles is determined by the total potential, generated by couplings that explicitly break the global symmetry SU(6). After turning on the γ, we can evaluate the potential in a new basis $\tilde{\Pi}(x)$, which is equivalent to a pNGB field redefinition,

$$\begin{aligned}\tilde{h} &= h\cos\gamma - \lambda_0\sin\gamma,\\ \tilde{\lambda}_0 &= h\sin\gamma + \lambda_0\cos\gamma,\end{aligned} \tag{5}$$

with the full mapping of other pNGBs provided in the Appendix A. We proved that, as expected, only tadpoles for $\tilde{h}$ (i.e., the Higgs) and $\tilde{\lambda}_0$ are generated. Furthermore, the tadpole terms from all contributions observe the same structure: $\frac{1}{f}\frac{\partial V_0(\alpha,\gamma)}{\partial\alpha}\tilde{h} - \frac{1}{v}\frac{\partial V_0(\alpha,\gamma)}{\partial\gamma}\tilde{\lambda}_0$, like the Taylor expansions. Thus, the vanishing of the tadpoles is guaranteed at the minimum of the potential. This is a main result of this paper and validates our choice for the vacuum misalignment in Eq. (4).

First, we study the potential V_0 coming from the top, gauge and underlying fermion mass, at $\gamma = 0$ as studied in [15]. The V_0 depends on 4 independent parameters: Q_A and R_S in the top sector, the underlying mass Bm (where B is a dimensionless form factor while m is the value of the underlying fermion mass), and a form factor for the gauge loops C_g. The Q_A represents the coupling of the quark doublet to top partner, and the R_S is the coupling of the quark singlet (a second parameter $R'_S \equiv rR_S$ is irrelevant to V_0). Although C_g and B can be computed on the lattice once an underlying dynamics is fixed, we will treat them as free parameters. The Q_A and R_S can be traded in terms of the misalignment angle α and the Higgs boson mass m_h:

$$\begin{aligned}Q_A^2 = \frac{m_h^2}{6v^2}\frac{\cos(2\alpha)}{\cos^2(\alpha)} - \frac{8\sqrt{2}Bm\sin(\alpha)}{3v}\\ - \frac{C_g g_2^2(\cos(2\theta_W)+2)}{3\cos^2(\theta_W)},\end{aligned} \tag{6}$$

$$R_S^2 = 4Q_A^2 + \frac{m_h^2}{2v^2}\sec^2(\alpha), \tag{7}$$

where $m_h = 125$ GeV is the measured Higgs mass.

We now introduce the masses for the light fermions via direct couplings. This means, in practice, that we introduce effective Yukawa couplings: e.g., for the bottom quark

$$-Y_b(\bar{q}_L b_R)\,\mathrm{Tr}[P\cdot\Sigma_{\alpha,\gamma}(x)] + \text{H.c.} \tag{8}$$

where Y_b is the Yukawa coupling and P is a matrix in the SU(6) space that extracts the Higgs components out of the pNGB matrix $\Sigma_{\alpha,\gamma}(x)$ [15]. Note that this kind of operators may also derive from partial compositeness upon integrating out the heavy partners of the light quarks. At one loop, this will generate a contribution to the potential for α and γ of the form

$$V_b \approx f^4 C_b|\mathrm{Tr}[P\cdot\Sigma_{\alpha,\gamma}(x)]|^2, \tag{9}$$

which generates a tadpole for $\tilde{\lambda}_0$ that does not vanish for $\gamma = 0$. More details on all potential contributions can be found in the Appendix A.

Expanding for small α and small γ, the cancellation of the tadpole $\frac{\partial V_0(\alpha,\gamma)}{\partial\gamma} = 0$ yields the following result

$$\gamma \simeq \frac{12\alpha m_b^2}{C_g m_W^2(72 + 40\tan^2(\theta_W)) + m_h^2}. \tag{10}$$

As a consequence of a nonvanishing γ, the model suffers from a tree-level correction to the ρ parameter:

$$\delta\rho_\gamma \simeq \frac{\sin^2(\gamma)+1}{(2\cos(2\alpha)+1)\sin^2(\gamma)+1} - 1. \tag{11}$$

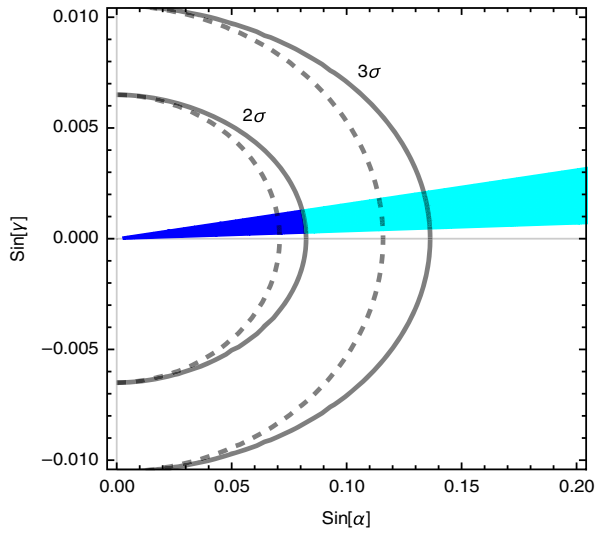

FIG. 1. EW precision bounds in the $\sin\alpha$-$\sin\gamma$ plane for model M3 (solid) and M4 (dashed). The blue wedge is the predicted region in the model, where the dark region is allowed at 2σ. We vary C_g between 0 (top edge) to 0.1 (bottom edge).

To study the impact of this correction, we determined the constraints from the EW precision tests, in the form of the oblique parameters S and T. Besides the tree-level correction, which impact directly T, we also included loops deriving from the modification of the Higgs couplings to gauge bosons, and a generic contribution to S from the strong sector. We thus define [29]

$$S = \frac{\sin^2\alpha}{6\pi}\left(\ln\frac{4\pi f}{m_h} + N_D\right), \tag{12}$$

$$T = -\frac{3\sin^2\alpha}{8\pi\cos^2\theta_W}\ln\frac{4\pi f}{m_h} + \frac{\delta\rho_\gamma}{\alpha_{\rm em}}, \tag{13}$$

where N_D counts the number of EW doublets in the underlying theory.

Numerically, we plot the bounds in Fig. 1 for two realistic models [16]: only two models are relevant, both based on a confining $\mathcal{G}_{\rm HC} = {\rm SO}(N_c)$, with $N_c = 7, 9$, and underlying fermions in the spinorial representation. Following the nomenclature of [30,31], we show M3 ($N_D = 16$) in solid and M4 ($N_D = 32$) in dashed. The blue-shaded wedge is the region or parameters spanned in our model, where we vary $0 < C_g < 0.1$. The plot shows that the value of γ is always very small, and that the bound on the parameter space is always dominated by the contribution of α to the S parameter. We should note that the generic contribution of the strong dynamics to the S parameter can be reduced in various way: replacing it by loops of the heavy states [32], considering a cancellation between vector and axial resonances [33], or including the effect of a lightish 0^{++} state [34]. For our purposes, the main point is to show that the effect of custodial breaking via γ is under control. We will not consider the bound on α from EW precision in the following because it can be reduced in a model-dependent way.

III. DARK MATTER PHENOMENOLOGY

Since the $\mathbb{Z}_2$-odd states in our model have sizable couplings to the SM, the relic abundance can be produced by the thermal freeze-out mechanism. We recall that the freeze-out temperature is typically a fraction of the DM mass, and that the DM mass in this model is always at most of the same order as the compositeness scale f. Thus, the calculations in this section can be performed within the range of validity of the effective theory, that is trustable up to $\Lambda_{\rm EFT} \sim 4\pi f$. The DM candidate(s) remain in thermal equilibrium with the SM, until the DM annihilation rate drops below the Hubble expansion rate. After the decoupling from the thermal bath (freeze-out), the DM density remains constant in a co-moving volume. Defining the yield $Y = n(x)/s(x)$, where $s(x)$ is the entropy density, the DM density evolution is described by the Boltzmann equation [35]:

$$\frac{dY}{dx} = -\frac{s(x=1)}{x^2 H(x=1)}\langle\sigma_{\rm eff} v\rangle[Y^2 - Y_{\rm eq}^2], \tag{14}$$

where

$$s(x=1) = \frac{2\pi^2}{45}g_* M^3, \quad H(x=1) = \sqrt{\frac{\pi^2}{90}g_*}\frac{M^2}{M_{\rm pl}}, \tag{15}$$

with $x = M/T$ and M being the DM mass. The effective thermal averaged cross section can normally be expanded as $\langle\sigma_{\rm eff} v\rangle = a^{(0)} + \frac{3}{2}a^{(1)}x^{-1} + \cdots$, unless the particle masses are near a threshold or a resonant regime [36]. Using an analytic approach, the relic density is calculated to be

$$\Omega h^2 = \frac{1.07\times 10^9\ {\rm GeV}^{-1}}{\sqrt{g_*(x_f)}M_{\rm pl}J(x_f)}, \quad J(x_f) = \int_{x_f}^{\infty} dx\frac{\langle\sigma_{\rm eff} v\rangle}{x^2}. \tag{16}$$

Assuming s-wave dominance for the annihilation cross-sections, the above equations yield an approximate solution $\langle\sigma_{\rm eff} v\rangle \simeq 2.0\times 10^{-26}\ {\rm cm}^3/s$ in order to saturate the relic density $\Omega h^2 = 0.12 \pm 0.001$ observed in the present Universe [1]. In the following we will use these results to calculate the favorable region of parameter space in our model.

Because of the DM parity described in Eq (2), all odd particles η_2 and $\phi_i = (A_0, H^0, H^\pm) \in H_2$ participate in the thermal equilibrium before the freeze-out. There exist a vertex of η_2-A_0-λ_0, thus via the Yukawa operators for the light quarks, the heavier component will quickly decay into the lightest mass eigenstate after freeze-out. In principal,

the effective averaged cross section need to take into account all co-annihilation processes [36,37].

However, the mass hierarchy in the spectrum is of paramount importance for co-annihilation. In our model, the inert Higgs doublet observes a mass hierarchy $m_{H_0} > m_{H^\pm} \gtrsim m_{A_0}$ [15]. In this work, we only investigate a simplified scenario $m_{A_0} > m_{\eta_2}$ with a large mass gap of $\Delta = (m_{A_0} - m_{\eta_2})/m_{\eta_2} > 0.2$, so that the actual DM is the singlet. At a typical freeze out temperature $x_f \sim 25$, the ratio of number densities, $n_{\phi_i}^{\rm eq}/n_{\eta_2}^{\rm eq}$, is highly suppressed by a Boltzmann factor $(1+\Delta)^{3/2}\exp(-\Delta x_f) \sim 1/200$. Since the direct annihilation $\langle\sigma_{\eta_2\eta_2} v\rangle$ is not subdominant, the co-annihilation effect can be safely neglected and one can only consider the direct annihilation of the singlet η_2. The dominant channels are

$$\begin{aligned}\langle\sigma_{\rm eff} v\rangle \simeq\ & \langle\sigma v(\eta_2\eta_2 \to VV)\rangle + \langle\sigma v(\eta_2\eta_2 \to hh)\rangle \\ & + \langle\sigma v(\eta_2\eta_2 \to \bar{f}f)\rangle + \langle\sigma v(\eta_2\eta_2 \to \eta_{p/m}\eta_{p/m})\rangle,\end{aligned} \tag{17}$$

where $\eta_{p/m}$ are linear combinations of the $\mathbb{Z}_2$-even $\eta_{1,3}$, which we should include because they are typically much lighter than other pNGBs and will eventually decay into SM particles [15]. The invariant cross section and the Møller velocity in the lab frame are

$$\begin{aligned}\sigma(\eta_2\eta_2 \to XY) =& \frac{1}{64\pi^2 s^{3/2}\sqrt{s-4m_\eta^2}} \int d\Omega |\bar{\mathcal{M}}_{XY}|^2 \\ & \times [s-(m_X+m_Y)^2]^{1/2}[s-(m_X-m_Y)^2]^{1/2},\end{aligned} \tag{18}$$

and

$$v_{\rm lab} = \sqrt{(p_a\cdot p_b)^2 - m_a^2 m_b^2}/(E_a E_b). \tag{19}$$

The amplitudes $|\bar{\mathcal{M}}_{XY}|^2$ are given in the Appendix B, as a function of all relevant couplings in the model. The key ingredient for relic density is the thermal averaged cross section, which can be evaluated by an integral (without velocity expansion of $\sigma v_{\rm lab}$) [38]:

$$\langle\sigma v_{\rm lab}\rangle = \frac{1}{8m_\eta^4 T K_2(x)^2}\int_{4m_\eta^2}^\infty ds\sigma\sqrt{s}(s-4m_\eta^2)K_1\left(\frac{\sqrt{s}}{T}\right), \tag{20}$$

with $K_{1,2}(x)$ being the modified Bessel functions of the second kind. In the region far from the resonance (Higgs mass), like the singlet DM with a mass of hundreds of GeV, the integral approach precisely matches with the s, p, and d-wave limits [39].

We now discuss the impact of direct detection experiments, which are sensitive to the recoil energy deposited by the scattering of DM to nucleus. In our model, the relevant interactions at the microscopic level are

$$\mathcal{L} \supset -\lambda_{h\eta_2^2} h\eta_2^2 - \lambda_{h\bar{q}q} h\bar{q}q + \frac{C_q m_q}{f^2}\eta_2^2\bar{q}q. \tag{21}$$

As already mentioned in the introduction, we work in the basis where derivative couplings of the DM candidate to a single Higgs boson are absent, thus all the above couplings explicitly break the shift symmetry associated with the Goldstone nature of the stable scalar. Besides the Higgs portal, we also have direct couplings to quarks from nonlinearities in the pNGB couplings (for light quarks, the last term comes from an effective Yukawa coupling). Thus, the spin-independent DM-nucleon cross section (factoring out $\frac{\mu_T^2}{\mu_N^2}A^2$ with respect to $\sigma^{\rm SI}_{\rm Nucleus}$) can be parameterized as [10,40]

$$\sigma_{\rm SI} = \frac{m_N^2}{\pi m_{\eta_2}^2}\left(\frac{m_N m_{\eta_2}}{m_N + m_{\eta_2}}\right)^2 \frac{(Zf_p + (A-Z)f_n)^2}{A^2}, \tag{22}$$

where $f_{p,n}$ characterize the interaction between η_2 and nucleons

$$f_{p,n} = \sum_q f_q^{(p,n)}\left[\frac{C_q}{f^2} + \frac{\lambda_{h\eta_2^2}}{v m_h^2}\right] \tag{23}$$

with q summing over all quark flavors. Note that setting $C_q = 0$ will exactly match the result in Ref. [41]. For the form factors $f_q^{(p,n)} = \frac{m_q}{m_N}\langle N|\bar{q}q|N\rangle$ [42], we will use the values from Ref. [43] for the light quarks, u, d, and s, while for heavy flavors the form factor can be computed via an effective coupling to gluons at one loop, giving

$$f_{c/b/t}^{(p,n)} = \frac{2}{27} f_{TG}^{(p,n)} = \frac{2}{27}\left(1 - \sum_{q=u,d,s} f_q^{(p,n)}\right). \tag{24}$$

For this model, the η_2 annihilation will mainly proceed in the following channels: $\eta_2\eta_2 \to W^+W^-, ZZ, hh, \bar{t}t, \bar{b}b$, and $\eta_{p,m}\eta_{p,m}$. The interactions and masses of pNGBs are determined by four parameters: (α, C_g, Bm, r), where we have neglected γ and set $\delta = 0$. The latter indicates a universal mass for all underlying fermions, and the δ only affects the mass splitting between η_p and η_m with minor impact on this analysis. Note that the r will influence the mass spectrum of DM parity odd particles $\eta_2, A_0, H_{0,\pm}$ but not others [15]. These parameters are preliminarily constrained by the nontachyon conditions, i.e., $m_\pi^2 > 0$ for all pNGBs.

In Fig. 2, we show the prospect for η_2 to play the role of DM, as opposed to the current bounds from direct

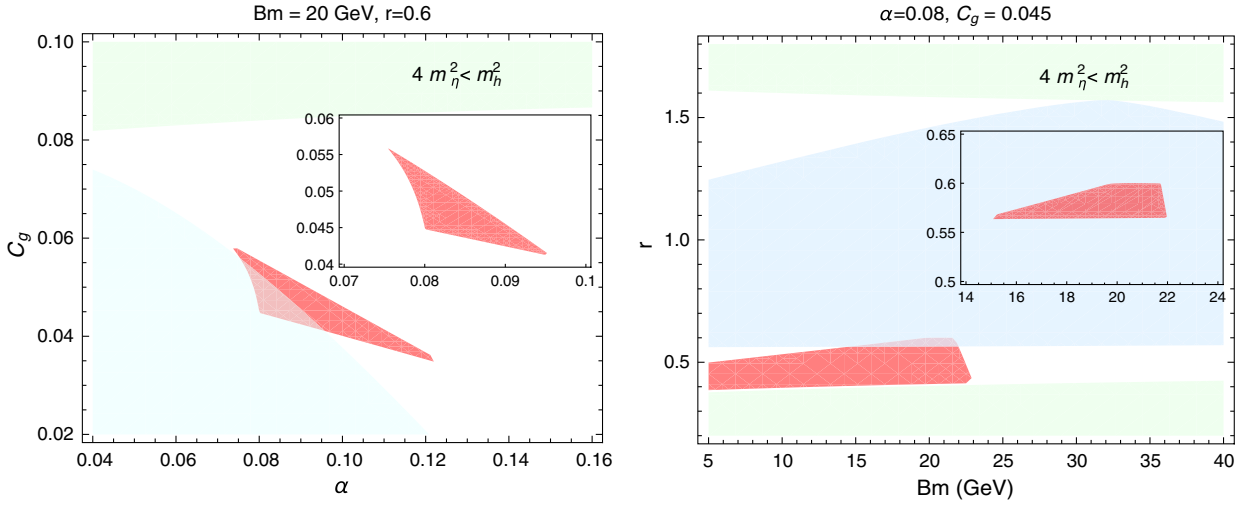

FIG. 2. The red wedge in these plots indicates the region satisfying the relic density bound $\Omega h^2 < 0.123$, along with nontachyon and negligible co-annihilation conditions imposed. The cyan bands are permitted by the direct detection bound while the green bands are the regions with $2m_\eta < m_h$ ($m_\eta^2 < 0$ included). The inset plots are the enlargements of regions that satisfy all the constraints.

detection. There is no constraint from the Higgs decay width since all singlet masses are heavier than m_h. For the two panels, we highlight the regions in red that satisfy the relic density bound $\Omega h^2 < 0.123$, as well as nontachyon conditions and $m_{A_0} > 1.2m_{\eta_2}$. While the light blue regions are permitted by the direct detection since we impose $\sigma_{\rm SI} < \sigma_{\rm SI}^{\rm exp}$. Only the overlaps between the red and blue are viable, where the relic density almost saturates $\Omega_{\eta_2} h^2 \sim 0.12$, thus it is not necessary to rescale $\sigma_{\rm SI}$ by a factor of $\Omega_{\eta_2}/\Omega_{\rm DM}$. The green regions indicate near the edge $2m_{\eta_2} = m_h$, the Higgs resonance is active, but they are far from the viable region, thus validating our analytical computation of the relic density. The region allowed by all the bounds, therefore, is fairly limited. Without fixing the parameters of (C_g, Bm), we get two branches centered around $(\alpha, r) \approx (0.08 \pm 0.01, 0.6 \pm 0.15)$ or $(0.02 \pm 0.01, 0.35 \pm 0.05)$, which implies $f \approx v/\alpha \sim 3.0$ or 12.0 TeV. We want to stress that the DM mass can be computed for each point of (α, C_g, Bm, r), so it varies over the slices of parameter space in the figure.

To better investigate the DM physics, we selected two illustrative benchmark points in Fig. 3: we show the thermal averaged cross section $\langle\sigma v\rangle$ for the $\bar{t}t$ channel and for the combined W^+W^-, ZZ, hh channels at $r = 0.4$ and $r = 0.6$ respectively, with $C_g = 0.05$ and $Bm = 20$ GeV fixed. Note that the intersection with the dashed green line indicates points saturating the observed relic density. We do not add the direct detection bound for Fig 3. For $r = 0.4$, the lower limit of m_{η_2} derives from the nontachyon condition, $m_{\eta_m}^2 > 0$, while the upper limit is bounded by the requirement of $m_{A_0} > 1.2m_{\eta_2}$. At this benchmark, the $\bar{t}t$ crosssection is dominant, reaching above 80% percent of the total contribution. The dot-dashed red line intersects with the reference cross section line for a DM mass of $m_{\eta_2} \sim 500$ GeV. Instead, for $r = 0.6$, the averaged cross section mainly comes from the combined dibosons and di-Higgs channels, with the blue solid line intersecting the reference value for a DM mass around $m_{\eta_2} \sim 700$ GeV. As inferred from Fig. 2, a smaller mass with a larger cross section is excluded by the direct detection. What this plot reveals is that due to the model-specific couplings, the DM cross section is dominated by the $\bar{t}t$ channel for lower masses, and by the diboson one for larger masses. For a

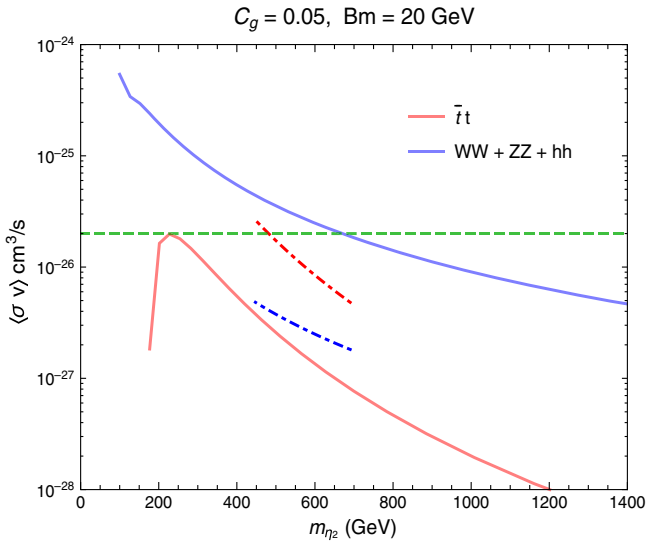

FIG. 3. Averaged cross section in the channels $\bar{t}t$ (red) and combined W^+W^-, ZZ, hh (blue) for two benchmark points with $r = 0.4$ (dashed) and $r = 0.6$ (solid) as a function of m_{η_2}. The dashed green line is the reference value $\langle\sigma v\rangle = 2.0 \times 10^{-26}$ cm^3/s for a relic density $\Omega h^2 \sim 0.12$.

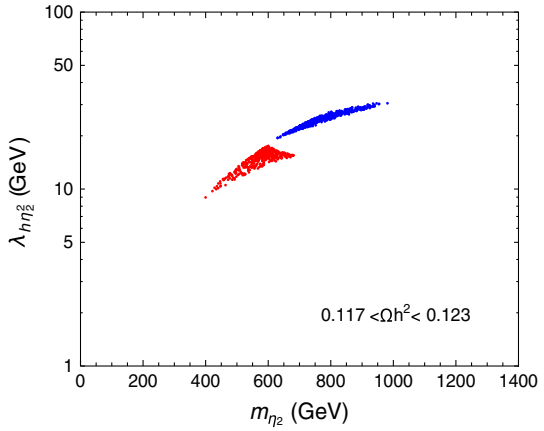

FIG. 4. Correlation between the Higgs portal coupling $\lambda_{h\eta^2}$ and the DM mass m_{η_2} after imposing all the necessary conditions, i.e., $0.117 < \Omega h^2 < 0.123$, nontachyon, negligible co-annihilation as well as direct detection bound. The red dots represent scenarios where the $\langle\sigma(\bar{t}t)v\rangle$ is dominant, while the blue dots stand for cases where the combined channels W^+W^-, ZZ, hh contribute the most.

further illustration, in Fig. 4, we show the results of a random scan of (α, C_g, Bm, r), where we retain only the points passing all the constraints, i.e., relic density, direct detection and no-tachyon conditions. As expected, we find two distinct branches of viable points: for $400 < m_{\eta_2} < 600$ GeV, the $\bar{t}t$ channel dominates, while for $600 < m_{\eta_2} < 1000$ GeV, it is the diboson W^+W^-, ZZ, hh that dominates the annihilation cross section. Note that this latter section is similar to the traditional Higgs portal singlet model. One new ingredient in our model is the annihilation into the lighter even pNGBs η_p and η_m: we have checked that this channel is always subleading, with a contribution of less that 3% for all points. Also, since the quartic couplings are relatively small, the cubic coupling $\lambda_{h\eta_2^2}$ is always close to the upper limit of the direct detection bound in order to put the relic density into the correct ballpark. This implies that the singlet DM candidate in our model is on the verge of being excluded by future direct detection experiments, like XENONnT [7] and LUX-ZEPLIN [44]. The projected sensitivity of the latter will improve the reach of the current XENON1T experiment by at least 1 order of magnitude. We found out that in such a situation there will be no overlap remaining in Fig. 2, and this DM scenario will be excluded. However, the same might not happen to the other DM candidate, i.e., A_0 in the inverted scenario of $m_{A_0} < m_{\eta_2}$. We leave this case for further investigation.

We should also consider the indirect detection signals, since the gamma ray line spectrum from the Galactic Center observed by Fermi-LAT and H.E.S.S. is possible to impose constraints for a DM mass in the interval of $(10, 10^3)$ GeV. According to the recent measurements, provided $400 < m_{\rm DM} < 1000$ GeV, the lowest upper limits on the DM annihilation cross section $\langle\sigma v\rangle$ for the $t\bar{t}$, W^+W^-, ZZ, and hh channels are around 10^{-25} cm$^3/s$ at $m_{\rm DM} \simeq 400$ GeV from Fermi-LAT [45] and 4.0×10^{-26} cm$^3/s$ at $m_{\rm DM} \simeq 1$ TeV from H.E.S.S [46]. In fact, the upper bounds in the mass region of interest $m_{\rm DM} \sim (400, 10^3)$ GeV, given by both telescopes from those concerning final states, are all well above the reference value 2.0×10^{-26} cm$^3/s$. This statement is consistent with the earlier analyses [47,48], where the relevant bounds are 1 order of magnitude larger. Thus in our model with the viable region almost saturating the relic density, the indirect detection can barely exclude any interesting parameter space. We would like to briefly comment on the collider phenomenology. Although the DM mass range is potentially accessible at colliders, including the LHC, the specific searches aiming at the DM pair production plus one additional SM particle are not available. As the masses are in the multihundred GeV ballpark, the pair production cross sections are very small and may only be accessible to the high luminosity run or at future high-energy colliders. The model also contains a light $\mathbb{Z}_2$-even pseudoscalar, whose mass can go down to 1 GeV. The collider phenomenology of this state has been discussed in Ref. [15].

IV. CONCLUSION

In this work, we analyzed the properties of a pseudoscalar singlet dark matter candidate that emerges as a pseudo-Nambu-Goldstone boson from a composite Higgs model, based on the coset SU(6)/SO(6). Since the light quarks, in particular the bottom, have to obtain their masses via an effective Yukawa operator originating from four fermion interaction, the custodial symmetry is unavoidably broken. We have proved that all the tadpole terms in a generic vacuum with (α, γ) angles will vanish after imposing the minimum conditions. More importantly, the γ value is suppressed by an order of m_b^2/m_h^2, making the custodial symmetry breaking well under control. Our result should also apply to the CHM model in SU(5)/SO(5), which shares the same bitriplet structure but without DM candidate.

Like most Higgs portal singlet models, the parameter space in this model is tightly constrained, mainly by direct detection experiments. Yet, due to the nonlinear nature of the DM couplings to the SM particles, we find that a small region of the parameter space is still allowed, with masses $400 < m_{\rm DM} < 1000$ GeV. For masses below ~600 GeV, the annihilation cross section is dominated by $\bar{t}t$, unlike the traditional models, while larger masses go back to dominant diboson channels. This pattern comes from the complicated pNGB couplings. Furthermore, requiring the correct relic density leaves the allowed regions within reach of future experiments, XENONnT and LUX-ZEPLIN, which might be able to exclude the η_2 as a DM.

Finally, the SU(6)/SO(6) model has another DM candidate in an inert second Higgs doublet, if it is lighter

than the singlet. The phenomenology of this state is similar to the traditional inert Higgs doublet model [49,50], which is also tightly constrained by observations. We leave an exploration of this limit for future work.

ACKNOWLEDGMENTS

G. C. acknowledges partial support from the Labex Lyon Institute of the Origins - LIO. The research of H. C. is supported by the Ministry of Science, ICT & Future Planning of Korea, the Pohang City Government, and the Gyeongsangbuk-do Provincial Government. H. C also acknowledges the support of TDLI during the revision of manuscript.

APPENDIX A: TADPOLE TERMS IN A GENERAL VACUUM

To ensure the DM stability, only two *CP*-even neutral pNGBs in this model, i.e., h and $\lambda_0 = -\frac{i}{\sqrt{2}}(\Lambda_0 - \Lambda_0^*)$ can develop VEVs. This means that we set $\beta = 0$ so that the second Higgs doublet remains inert. The pNGB matrix is parametrized as

$$\begin{aligned}\Sigma_{\alpha,\gamma}(x) &= U(\alpha,\gamma)\cdot\Sigma(x)\cdot U^T(\alpha,\gamma)\\ &= U(\alpha,\gamma)\cdot e^{i\frac{2\sqrt{2}}{f}\Pi(x)}\cdot\Sigma_{\rm EW}\cdot U^T(\alpha,\gamma),\end{aligned}\tag{A1}$$

where the $\Sigma_{\rm EW}$ is rotated away to be misaligned with the direction of $\mathrm{SU}(2)_L \times U(1)_Y$ by $\mathrm{U}(\alpha,\gamma)$. In analogy to the β rotation, the SU(6) transformation can be decomposed into

$$U(\alpha,\gamma) = U_\gamma \cdot U_\alpha \cdot U_\gamma^\dagger = e^{i\gamma\sqrt{2}S_8}\cdot e^{i\alpha\sqrt{2}X_{10}}\cdot e^{-i\gamma\sqrt{2}S_8}\tag{A2}$$

with $U_\gamma = e^{i\gamma\sqrt{2}S_8}$ defined in term of an unbroken generator. The inner $U_\gamma^\dagger$ operation on $\Sigma(x)$ can be fully absorbed by the pNGB field redefinition. Thus it is the outer U_γ that determines the γ dependence. And Eq. (A1) can be rewritten as

$$\begin{aligned}\Sigma_{\alpha,\gamma}(x) &= U_\gamma\cdot U_\alpha\cdot\tilde{\Sigma}(x)\cdot U_\alpha^T\cdot U_\gamma^T\\ &= U_\gamma\cdot U_\alpha\cdot e^{i\frac{2\sqrt{2}}{f}\tilde{\Pi}(x)}\cdot\Sigma_{\rm EW}\cdot U_\alpha^T\cdot U_\gamma^T.\end{aligned}\tag{A3}$$

with $\tilde{\Sigma}(x) = U_\gamma^\dagger\cdot\Sigma(x)\cdot U_\gamma^*$. Thus we can find out an exact mapping for $\Pi(x)\to\tilde{\Pi}(x)$ in terms of pNGB fields. The field redefinition can be split into several blocks and leaving the pion fields $H_{\pm,0}$ unchanged. For h and λ_0, they transform in a SO(2) rotation defined by γ:

$$\begin{aligned}\tilde{h} &= h\cos(\gamma) - \lambda_0\sin(\gamma),\\ \tilde{\lambda}_0 &= h\sin(\gamma) + \lambda_0\cos(\gamma).\end{aligned}\tag{A4}$$

This also applies to the DM candidates A_0 and η_2:

$$\begin{aligned}\tilde{A}_0 &= A_0\cos(\gamma) - \eta_2\sin(\gamma),\\ \tilde{\eta}_2 &= \eta_2\cos(\gamma) + A_0\sin(\gamma).\end{aligned}\tag{A5}$$

The charged Goldstone G_+ eaten by W^+ can mix with the Λ_+ and ϕ_+ in the bitriplet.

$$\begin{aligned}\tilde{\Lambda}_+ &= \Lambda_+\cos^2\left(\frac{\gamma}{2}\right) - \varphi_+\sin^2\left(\frac{\gamma}{2}\right) - \frac{i}{\sqrt{2}}G_+\sin(\gamma),\\ \tilde{\varphi}_+ &= \varphi_+\cos^2\left(\frac{\gamma}{2}\right) - \Lambda_+\sin^2\left(\frac{\gamma}{2}\right) - \frac{i}{\sqrt{2}}G_+\sin(\gamma),\\ \tilde{G}_+ &= G_+\cos(\gamma) - \frac{i}{\sqrt{2}}(\Lambda_+ + \varphi_+)\sin(\gamma).\end{aligned}\tag{A6}$$

Finally, the neutral Goldstone G_0 mixes with $\eta_{1,3}$, λ, and φ_0 under the γ rotation. With the definition $\eta_G \equiv \frac{1}{2\sqrt{2}}(\sqrt{3}\eta_1 - \sqrt{2}\eta_3 + \sqrt{2}\lambda - \varphi_0)$, we can obtain

$$\begin{aligned}\tilde{G}_0 &= G_0\cos(2\gamma) - \eta_G\sin(2\gamma),\\ \tilde{\eta}_1 &= \eta_1 - \frac{1}{2}\sqrt{\frac{3}{2}}(2\eta_G\sin^2(\gamma) - G_0\sin(2\gamma)),\\ \tilde{\eta}_3 &= \eta_3 + \frac{1}{2}(2\eta_G\sin^2(\gamma) - G_0\sin(2\gamma)),\\ \tilde{\lambda} &= \lambda - \frac{1}{2}(2\eta_G\sin^2(\gamma) - G_0\sin(2\gamma)),\\ \tilde{\varphi}_0 &= \varphi_0 + \frac{1}{2\sqrt{2}}(2\eta_G\sin^2(\gamma) - G_0\sin(2\gamma)).\end{aligned}\tag{A7}$$

Note that the last four expressions in Eq. (A7) give: $\tilde{\eta}_G = \eta_G\cos(2\gamma) + G_0\sin(2\gamma)$, explicitly orthogonal to $\tilde{G}_0$. It turns out to be easier to calculate the potentials in the new basis of $\tilde{\Pi}(x)$. We can demonstrate that for each type of potential in a generic vacuum with (α,γ) angles, the coefficient of $\tilde{h}$ tadpole term is equal to $\frac{1}{f}\frac{\partial V_0(\alpha,\gamma)}{\partial\alpha}$, while the coefficient of $\tilde{\lambda}_0$ tadpole term is equal to $-\frac{1}{v}\frac{\partial V_0(\alpha,\gamma)}{\partial\gamma}$.

1. The gauge potential

$$V_g = \frac{C_g}{4}f^4(g_2^2\mathrm{Tr}[T_L^i\Sigma(T_L^i\Sigma)^*] + g_1^2\mathrm{Tr}[Y\Sigma(Y\Sigma)^*]).\tag{A8}$$

Expand the pion matrix, the vacuum term at the lowest order is

$$\begin{aligned}\mathcal{V}_{g,0}(\alpha,\gamma) = -\frac{C_g f^4}{32}&(4\sin^2(\alpha)\cos(2\gamma)(2\cos(2\alpha)(g_1^2+g_2^2)\\ &+ g_1^2 + 3g_2^2) + 2\cos(2\alpha)(g_1^2+7g_2^2)\\ &+ 2\cos(4\alpha)(g_1^2+g_2^2) + 4(g_1^2+2g_2^2)).\end{aligned}\tag{A9}$$

The tadpole terms are obtained by expanding until the linear order:

$$V_g(\tilde{h}) = \frac{C_g f^3}{8}(4\sin(4\alpha)\sin^2(\gamma)(g_1^2+g_2^2)+\sin(2\alpha)(g_1^2+7g_2^2+\cos(2\gamma)(g_1^2-g_2^2)))\tilde{h}$$
$$= \frac{1}{f}\frac{\partial \mathcal{V}_{g,0}(\alpha,\gamma)}{\partial\alpha}\tilde{h}. \tag{A10}$$

$$V_g(\tilde{\lambda}_0) = -\frac{C_g}{4}f^3\sin(\alpha)\sin(2\gamma)(2\cos(2\alpha)(g_1^2+g_2^2)+g_1^2+3g_2^2)\tilde{\lambda}_0$$
$$= -\frac{1}{f\sin\alpha}\frac{\partial \mathcal{V}_{g,0}(\alpha,\gamma)}{\partial\gamma}\tilde{\lambda}_0 = -\frac{1}{v}\frac{\partial \mathcal{V}_{g,0}(\alpha,\gamma)}{\partial\gamma}\tilde{\lambda}_0. \tag{A11}$$

2. The bottom Yukawa potential

$$V_b = C_b f^4 \sum_\delta |Y_{b1}\mathrm{Tr}[P^\delta_{b1}.\Sigma(x)] + Y_{b2}\mathrm{Tr}[P^\delta_{b2}.\Sigma(x)]|^2. \tag{A12}$$

The vacuum term is

$$\mathcal{V}_{b,0}(\alpha,\gamma) = 2C_b f^4 Y_{\mathrm{b1}}(Y_{\mathrm{b1}})^*\sin^2(\alpha)\cos^2(\gamma)(\cos(\alpha)-\sin(\alpha)\sin(\gamma))^2. \tag{A13}$$

The tadpoles terms are

$$V_b(\tilde{h}) = 4C_b f^3 Y_{\mathrm{b1}}(Y_{\mathrm{b1}})^*\sin(\alpha)\cos^2(\gamma)(\cos(\alpha)-\sin(\alpha)\sin(\gamma))(\cos(2\alpha)-\sin(2\alpha)\sin(\gamma))\tilde{h}$$
$$= \frac{1}{f}\frac{\partial \mathcal{V}_{b,0}(\alpha,\gamma)}{\partial\alpha}\tilde{h}. \tag{A14}$$

$$V_b(\tilde{\lambda}_0) = 4C_b f^3 Y_{\mathrm{b1}}(Y_{\mathrm{b1}})^*\sin(\alpha)\cos(\gamma)(\sin(\alpha)\cos(2\gamma)+\cos(\alpha)\sin(\gamma))(\cos(\alpha)-\sin(\alpha)\sin(\gamma))\tilde{\lambda}_0$$
$$= -\frac{1}{v}\frac{\partial \mathcal{V}_{b,0}(\alpha,\gamma)}{\partial\gamma}\tilde{\lambda}_0. \tag{A15}$$

3. The top spurion potential

$$V_t = \frac{C_{LL}f^4}{4}\mathrm{Tr}[\bar{D}_L^T\cdot\Sigma^\dagger\cdot D_L\cdot\Sigma] + \frac{C_{RR}f^4}{4}\mathrm{Tr}[\bar{D}_R^T\cdot\Sigma^\dagger\cdot D_R\cdot\Sigma]. \tag{A16}$$

Setting $C_{LL} = C_{RR} = 1$, the vacuum term is

$$\mathcal{V}_{t,0} = \frac{f^4}{16}(2\sin^2(\alpha)(2\cos(2\alpha)+3)\cos(2\gamma)-5\cos(2\alpha)-\cos(4\alpha)-2)|Q_A|^2$$
$$+\frac{f^4}{256}(8\cos(4\alpha)\cos^4(\gamma)+8\cos(2\alpha)\sin^2(2\gamma)-4\cos(2\gamma)+3\cos(4\gamma))|R_S|^2 + \text{Constant Term}. \tag{A17}$$

The tadpole terms are

$$V_t(\tilde{h}) = \frac{f^3}{16}\sin(\alpha)\cos(\alpha)(4(8\cos(2\alpha)\cos^2(\gamma)+\cos(2\gamma)+5)|Q_A|^2+|R_S|^2(-8\cos(2\alpha)\cos^4(\gamma)+\cos(4\gamma)-1))\tilde{h}$$
$$= \frac{1}{f}\frac{\partial \mathcal{V}_{t,0}(\alpha,\gamma)}{\partial\alpha}\tilde{h}. \tag{A18}$$

$$V_t(\tilde{\lambda}_0) = \frac{f^3}{4}\sin(\alpha)\sin(2\gamma)((2\cos(2\alpha)+3)|Q_A|^2+|R_S|^2(\sin^2(\alpha)\cos(2\gamma)-\cos^2(\alpha)))\tilde{\lambda}_0$$
$$= -\frac{1}{v}\frac{\partial \mathcal{V}_{t,0}(\alpha,\gamma)}{\partial\gamma}\tilde{\lambda}_0. \tag{A19}$$

4. The mass term potential

$$V_m = -\frac{Bf^3}{2\sqrt{2}}\mathrm{Tr}[M^\dagger \cdot \Sigma] + \mathrm{H.c.} \tag{A20}$$

with

$$M = \begin{pmatrix} & im_2\sigma_2 & \\ -im_2\sigma_2 & & \\ \hline & & m_1\mathbb{1}_2 \end{pmatrix}, \tag{A21}$$

for $m_1 = m_2$, the mass matrix M is aligned with Σ_{EW}. First the vacuum term in the general case is

$$\mathcal{V}_{m,0} = \frac{Bf^3}{2\sqrt{2}}(m_2(2\sin^2(\alpha)\cos(2\gamma) + 3\cos(2\alpha) + 5) - m_1(2\sin^2(\alpha)\cos(2\gamma) - \cos(2\alpha) - 3)). \tag{A22}$$

The tadpole terms read

$$\begin{aligned} V_m(\tilde{h}) &= \frac{Bf^2}{\sqrt{2}}\sin(2\alpha)(m_2(\cos(2\gamma) - 3) - 2m_1\cos^2(\gamma))\tilde{h} \\ &= \frac{1}{f}\frac{\partial \mathcal{V}_{m,0}(\alpha,\gamma)}{\partial\alpha}\tilde{h}. \end{aligned} \tag{A23}$$

$$\begin{aligned} V_m(\tilde{\lambda}_0) &= Bf^2\sqrt{2}(m_2 - m_1)\sin(\alpha)\sin(2\gamma)\tilde{\lambda}_0 \\ &= -\frac{1}{v}\frac{\partial \mathcal{V}_{m,0}(\alpha,\gamma)}{\partial\gamma}\tilde{\lambda}_0. \end{aligned} \tag{A24}$$

We can see for $m_1 = m_2$, there is no γ dependence in the $\tilde{h}$ and $\tilde{\lambda}_0$ basis because $U_\gamma^T \cdot M \cdot U_\gamma = M$ holds true. The explicit symmetry breaking is $\mathrm{SU}(6) \to \mathrm{SO}(6)$ and the potential is equivalent to the one in an α vacuum.

Note that only for the bottom Yukawa potential, the tadpole term of $\tilde{\lambda}_0$ is proportional to $\cos(\gamma)$, thus nonvanishing at $\gamma = 0$; but for the other potentials, the tadpole term of $\tilde{\lambda}_0$ is proportional to $\sin(2\gamma)$. Furthermore, if we change $\gamma \to -\gamma$, the minus sign for the $\tilde{\lambda}$ tadpole term will be flipped so that $V(\tilde{\lambda}_0) = \frac{1}{v}\frac{\partial V_0(\alpha,\gamma)}{\partial\gamma}\tilde{\lambda}_0$.

APPENDIX B: THE ANNIHILATION AMPLITUDES

Here we give all the amplitudes squared used for the relic density calculation:

$$|\bar{\mathcal{M}}(\eta_2\eta_2 \to W^+W^-)|^2 = \frac{e^4(12M_W^4 - 4M_W^2 s + s^2)}{16M_W^4 S_W^4(\Gamma_h^2 m_h^2 + (m_h^2 - s)^2)}((2v\cos(\alpha)\lambda_{h\eta_2^2} + \sin^2(\alpha)(m_h^2 - s))^2 + \Gamma_h^2 m_h^2 \sin^4(\alpha)). \tag{B1}$$

$$|\bar{\mathcal{M}}(\eta_2\eta_2 \to ZZ)|^2 = \frac{e^4(12M_Z^4 - 4M_Z^2 s + s^2)}{16C_W^4 S_W^4 M_Z^4(\Gamma_h^2 m_h^2 + (m_h^2 - s)^2)}((2v\cos(\alpha)\lambda_{h\eta_2^2} + \sin^2(\alpha)(m_h^2 - s))^2 + \Gamma_h^2 m_h^2 \sin^4(\alpha)). \tag{B2}$$

$$|\bar{\mathcal{M}}(\eta_2\eta_2 \to \bar{t}t)|^2 = \frac{24(s - 4m_t^2)}{v^2(\Gamma_h^2 m_h^2 + (m_h^2 - s)^2)}\left(\left(\frac{m_t\cos(4\alpha)}{\cos(2\alpha)\cos(\alpha)}\lambda_{h\eta_2^2} + v(m_h^2 - s)\lambda_{\eta_2^2 t^2}\right)^2 + \Gamma_h^2 m_h^2 v^2 \lambda_{\eta_2^2 t^2}^2\right). \tag{B3}$$

$$|\bar{\mathcal{M}}(\eta_2\eta_2 \to \bar{b}b)|^2 = \frac{24(s - 4m_b^2)}{v^2(\Gamma_h^2 m_h^2 + (m_h^2 - s)^2)}\left(\left(\frac{m_b\cos(2\alpha)}{\cos(\alpha)}\lambda_{h\eta_2^2} + v(m_h^2 - s)\lambda_{\eta_2^2 b^2}\right)^2 + \Gamma_h^2 m_h^2 v^2 \lambda_{\eta_2^2 b^2}^2\right). \tag{B4}$$

$$|\bar{\mathcal{M}}(\eta_2\eta_2 \to hh)|^2 = 4\Bigg(4\lambda^2_{h^2\eta_2^2} + \frac{64\lambda^4_{h\eta_2^2}(s-2m_h^2)^2}{(\cos^2(\theta)(4m_h^2-s)(s-4m_\eta^2)+(s-2m_h^2)^2)^2} + \frac{12m_h^2\cos(2\alpha)\ \sec(\alpha)\lambda_{h^2\eta_2^2}\lambda_{h\eta_2^2}(s-m_h^2)}{v(\Gamma_h^2m_h^2+(m_h^2-s)^2)} + \frac{9\lambda^2_{h\eta_2^2}m_h^4\cos^2(2\alpha)\ \sec^2(\alpha)}{v^2(\Gamma_h^2m_h^2+(m_h^2-s)^2)} - \frac{48m_h^2\cos(2\alpha)\ \sec(\alpha)\lambda^3_{h\eta_2^2}(2m_h^4-3m_h^2s+s^2)}{v(\Gamma_h^2m_h^2+(m_h^2-s)^2)(\cos^2(\theta)(4m_h^2-s)(s-4m_\eta^2)+(s-2m_h^2)^2)} + \frac{32\lambda^2_{h\eta_2^2}\lambda_{h^2\eta_2^2}(2m_h^2-s)}{\cos^2(\theta)(4m_h^2-s)(s-4m_\eta^2)+(s-2m_h^2)^2}\Bigg). \tag{B5}$$

$$|\bar{\mathcal{M}}(\eta_2\eta_2 \to \eta_m\eta_m)|^2 = 16\Bigg(\lambda^2_{\eta_2^2\eta_m^2} + \frac{(\lambda^2_{h\eta_m^2}\lambda^2_{h\eta_2^2} + 2\lambda_{\eta_2^2\eta_m^2}\lambda_{h\eta_m^2}\lambda_{h\eta_2^2}(s-m_h^2))}{\Gamma_h^2m_h^2+(m_h^2-s)^2}\Bigg). \tag{B6}$$

$$|\bar{\mathcal{M}}(\eta_2\eta_2 \to \eta_p\eta_m)|^2 = 4\Bigg(\lambda^2_{\eta_2^2\eta_p\eta_m} + \frac{(\lambda^2_{h\eta_m\eta_p}\lambda^2_{h\eta_2^2} + 2\lambda_{\eta_2^2\eta_p\eta_m}\lambda_{h\eta_p\eta_m}\lambda_{h\eta_2^2}(s-m_h^2))}{\Gamma_h^2m_h^2+(m_h^2-s)^2}\Bigg). \tag{B7}$$

For $|\bar{\mathcal{M}}(\eta_2\eta_2 \to \eta_p\eta_p)|^2$, we can simply replace $\lambda_{h\eta_m^2} \to \lambda_{h\eta_p^2}$ and $\lambda_{\eta_2^2\eta_m^2} \to \lambda_{\eta_2^2\eta_p^2}$ in Eq. (B6).

APPENDIX C: THE VERTICES

The Lagrangian relevant to DM annihilations can be written as three parts: $\mathcal{L} = \mathcal{L}_V + \mathcal{L}_S + \mathcal{L}_f$:

$$\mathcal{L}_V = \frac{g^2}{8}(2hv\cos(\alpha) - \eta_2^2\sin^2(\alpha))(2W_\mu^-W_\mu^+ + Z_\mu^2\sec^2(\theta_w)), \tag{C1}$$

$$\mathcal{L}_S = -(\lambda_{h^2\eta_2^2}h^2 + \lambda_{\eta_m^2\eta_2^2}\eta_m^2 + \lambda_{\eta_p\eta_m\eta_2^2}\eta_m\eta_p + \lambda_{\eta_p^2\eta_2^2}\eta_p^2)\eta_2^2 - (\lambda_{h\eta_2^2}\eta_2^2 + \lambda_{h\eta_p^2}\eta_p^2 + \lambda_{h\eta_m^2}\eta_m^2 + +\lambda_{h\eta_p\eta_m}\eta_p\eta_m)h - \frac{m_h^2\cos(2\alpha)\ \sec(\alpha)}{2v}h^3, \tag{C2}$$

$$\mathcal{L}_f = -\frac{4m_t\cos(4\alpha)}{f\sin(4\alpha)}h\bar{t}t - \frac{2m_b\cos(2\alpha)}{f\sin(2\alpha)}h\bar{b}b + \lambda_{\eta_2^2\bar{t}t}\eta_2^2\bar{t}t + \lambda_{\eta_2^2\bar{b}b}\eta_2^2\bar{b}b, \tag{C3}$$

where those λ couplings are complicated functions of (α, C_g, Bm, r), imposed by the minimum $\frac{\partial V_0(\alpha)}{\partial\alpha} = 0$ and Higgs mass conditions after extraction from the potentials. We explicitly list their expressions as the following:

$$\lambda_{h^2\eta_2^2} = \Bigg(\frac{m_h^2\sec^2(\alpha)}{144v^2}((8r^2-50r+20)\cos(2\alpha) + 6r^2 + 7(5-4r)\cos(4\alpha) - 34r + 11) + \frac{2\sqrt{2}Bm}{9v}(2r-1)\sin(\alpha)(14\cos(2\alpha) - 2r + 1) + \frac{2\mathrm{Cg}M_w^2}{9v^2}(7(2r-1)\cos(2\alpha) - 2(r-1)r + 1)(\cos(2\theta_W) + 2)\sec^2(\theta_W)\Bigg). \tag{C4}$$

$$\lambda_{h\eta_2^2} = \Bigg(\frac{m_h^2\sec(\alpha)}{12v}((7-8r)\cos(2\alpha) + 3 - 6r) + \frac{2C_gM_w^2}{3v}\cos(\alpha)(16r - 7 + (8r-5)\cos(2\theta_W))\sec^2(\theta_W) + \frac{8}{3}\sqrt{2}Bm(2r-1)\sin(2\alpha)\Bigg). \tag{C5}$$

$$\lambda_{\eta_2^2\eta_m^2} = \Big(-\frac{m_h^2\sec^2(\alpha)}{2880v^2}((64(7-4r)r+636)\cos(2\alpha)+(128r+41)\cos(4\alpha)+64(5-3r)r+251)$$
$$+\frac{4C_gM_w^2}{45v^2}((8r-4)\cos(2\alpha)-8(r-1)r+39)(\cos(2\theta_W)+2)\sec^2(\theta_W)$$
$$+\frac{\sqrt{2}B_m\sin(\alpha)}{45v}((64r+25)\cos(2\alpha)-64(r-1)r+159)\Big). \tag{C6}$$

$$\lambda_{\eta_2^2\eta_p^2} = \Big(\frac{m_h^2\sec^2(\alpha)}{30v^2}((r(4r-7)+1)\cos(2\alpha)+(1-2r)\cos(4\alpha)+r(3r-5)+1)$$
$$+\frac{8C_gM_w^2}{15v^2}((2r-1)\cos(2\alpha)-2(r-1)r+1)(\cos(2\theta_W)+2)\sec^2(\theta_W)$$
$$+\frac{2\sqrt{2}Bm\sin(\alpha)}{15v}((16r-5)\cos(2\alpha)-16(r-1)r-9)\Big). \tag{C7}$$

$$\lambda_{\eta_2^2\eta_m\eta_p} = \Big(\frac{m_h^2\sec^2(\alpha)}{120\sqrt{6}v^2}(-4(4r(4r-7)+29)\cos(2\alpha)+(32r-31)\cos(4\alpha)+16(5-3r)r-61)$$
$$+\frac{16\sqrt{\frac{2}{3}}C_g\mathrm{Mw}^2}{15v^2}((1-2r)\cos(2\alpha)+2((r-1)r+2))(\cos(2\theta_W)+2)\sec^2(\theta_W)$$
$$+\frac{8B_m\sin(\alpha)}{15\sqrt{3}v}((15-16r)\cos(2\alpha)+16(r-1)r+19)\Big). \tag{C8}$$

$$\lambda_{h\eta_m^2} = \frac{8}{5}\sqrt{2}Bm\ \sin(2\alpha)\lambda_{h\eta_p\eta_m} = \frac{4}{5}\sqrt{3}Bm\ \sin(2\alpha). \tag{C9}$$

$$\lambda_{h\eta_p^2} = -\frac{4}{15}\sqrt{2}Bm\ \sin(2\alpha) \qquad \lambda_{\eta_2^2\bar{b}b} = \frac{m_b\sin^2(\alpha)}{v^2}. \tag{C10}$$

$$\lambda_{\eta_2^2\bar{t}t} = \frac{m_t\sin^2(\alpha)(2\cos(2\alpha)-2r+1)}{v^2\cos(2\alpha)}. \tag{C11}$$

[1] N. Aghanim *et al.* (Planck Collaboration), Astron. Astrophys. **641**, A6 (2020).
[2] V. Silveira and A. Zee, Phys. Lett. **161B**, 136 (1985).
[3] J. McDonald, Phys. Rev. D **50**, 3637 (1994).
[4] C. Burgess, M. Pospelov, and T. ter Veldhuis, Nucl. Phys. **B619**, 709 (2001).
[5] J. A. Casas, D. G. Cerdeno, J. M. Moreno, and J. Quilis, J. High Energy Phys. 05 (2017) 036.
[6] G. Arcadi, A. Djouadi, and M. Raidal, Phys. Rep. **842**, 1 (2020).
[7] E. Aprile *et al.* (XENON Collaboration), Phys. Rev. Lett. **121**, 111302 (2018).
[8] X. Cui *et al.* (PandaX-II Collaboration), Phys. Rev. Lett. **119**, 181302 (2017).
[9] D. Akerib *et al.* (LUX Collaboration), Phys. Rev. Lett. **118**, 021303 (2017).
[10] M. Frigerio, A. Pomarol, F. Riva, and A. Urbano, J. High Energy Phys. 07 (2012) 015.
[11] J. Galloway, J. A. Evans, M. A. Luty, and R. A. Tacchi, J. High Energy Phys. 10 (2010) 086.
[12] R. Balkin, M. Ruhdorfer, E. Salvioni, and A. Weiler, J. Cosmol. Astropart. Phys. 11 (2018) 050.
[13] C. Gross, O. Lebedev, and T. Toma, Phys. Rev. Lett. **119**, 191801 (2017).
[14] G. Cacciapaglia, C. Pica, and F. Sannino, Phys. Rep. **877**, 1 (2020).
[15] G. Cacciapaglia, H. Cai, A. Deandrea, and A. Kushwaha, J. High Energy Phys. 10 (2019) 035.
[16] G. Ferretti and D. Karateev, J. High Energy Phys. 03 (2014) 077.
[17] M. J. Dugan, H. Georgi, and D. B. Kaplan, Nucl. Phys. **B254**, 299 (1985).

[18] H. Georgi and M. Machacek, Nucl. Phys. **B262**, 463 (1985).
[19] A. Agugliaro, G. Cacciapaglia, A. Deandrea, and S. De Curtis, J. High Energy Phys. 02 (2019) 089.
[20] D. Marzocca and A. Urbano, J. High Energy Phys. 07 (2014) 107.
[21] Y. Wu, T. Ma, B. Zhang, and G. Cacciapaglia, J. High Energy Phys. 11 (2017) 058.
[22] G. Ballesteros, A. Carmona, and M. Chala, Eur. Phys. J. C **77**, 468 (2017).
[23] R. Balkin, M. Ruhdorfer, E. Salvioni, and A. Weiler, J. High Energy Phys. 11 (2017) 094.
[24] R. Balkin, G. Perez, and A. Weiler, Eur. Phys. J. C **78**, 104 (2018).
[25] T. Alanne, M. Heikinheimo, V. Keus, N. Koivunen, and K. Tuominen, Phys. Rev. D **99**, 075028 (2019).
[26] C. Cai, H.-H. Zhang, G. Cacciapaglia, M. T. Frandsen, and M. Rosenlyst, Phys. Rev. Lett. **125**, 021801 (2020).
[27] M. Ramos, J. High Energy Phys. 07 (2020) 128.
[28] H. Georgi and D. B. Kaplan, Phys. Lett. **145B**, 216 (1984).
[29] A. Arbey, G. Cacciapaglia, H. Cai, A. Deandrea, S. Le Corre, and F. Sannino, Phys. Rev. D **95**, 015028 (2017).
[30] A. Belyaev, G. Cacciapaglia, H. Cai, G. Ferretti, T. Flacke, A. Parolini, and H. Serodio, J. High Energy Phys. 01 (2017) 094; 12 (2017) 088(E).
[31] G. Cacciapaglia, G. Ferretti, T. Flacke, and H. Serôdio, Front. Phys. **7**, 22 (2019).
[32] D. Ghosh, M. Salvarezza, and F. Senia, Nucl. Phys. **B914**, 346 (2017).
[33] J. Hirn and V. Sanz, Phys. Rev. Lett. **97**, 121803 (2006).
[34] D. Buarque Franzosi, G. Cacciapaglia, and A. Deandrea, Eur. Phys. J. C **80**, 28 (2020).
[35] E. W. Kolb and M. S. Turner, *The Early Universe*, Frontiers in Physics, 1st ed. (Westview Press, 1990), p. 596, https://doi.org/10.1201/9780429492860.
[36] K. Griest and D. Seckel, Phys. Rev. D **43**, 3191 (1991).
[37] J. Edsjo and P. Gondolo, Phys. Rev. D **56**, 1879 (1997).
[38] P. Gondolo and G. Gelmini, Nucl. Phys. **B360**, 145 (1991).
[39] M. Srednicki, R. Watkins, and K. A. Olive, Nucl. Phys. **B310**, 693 (1988).
[40] T. Han and R. Hempfling, Phys. Lett. B **415**, 161 (1997).
[41] J. M. Cline, K. Kainulainen, P. Scott, and C. Weniger, Phys. Rev. D **88**, 055025 (2013); **92**, 039906(E) (2015).
[42] M. Drees and M. Nojiri, Phys. Rev. D **48**, 3483 (1993).
[43] H.-Y. Cheng and C.-W. Chiang, J. High Energy Phys. 07 (2012) 009.
[44] D. Akerib *et al.* (LUX-ZEPLIN Collaboration), Phys. Rev. D **101**, 052002 (2020).
[45] M. Ackermann *et al.* (Fermi-LAT Collaboration), Phys. Rev. Lett. **115**, 231301 (2015).
[46] H. Abdallah *et al.* (H.E.S.S. Collaboration), Phys. Rev. Lett. **117**, 111301 (2016).
[47] K. N. Abazajian, P. Agrawal, Z. Chacko, and C. Kilic, J. Cosmol. Astropart. Phys. 11 (2010) 041.
[48] K. N. Abazajian, S. Blanchet, and J. Harding, Phys. Rev. D **85**, 043509 (2012).
[49] A. Belyaev, G. Cacciapaglia, I. P. Ivanov, F. Rojas-Abatte, and M. Thomas, Phys. Rev. D **97**, 035011 (2018).
[50] L. Lopez Honorez, E. Nezri, J. F. Oliver, and M. H. Tytgat, J. Cosmol. Astropart. Phys. 02 (2007) 028.